Integral berthing with non-cooperative targets through a pseudospectral, shape-based solver and MPC

Sergio Cuevas del Valle, Ester Velázquez Navarro, Hodei Urrutxua, Pablo Solano-López

Aerospace Systems and Transport Research Group, University Rey Juan Carlos, Camino del Molino 5, 28942, Fuenlabrada, Spain
s.cuevas.2017@alumnos.urjc.es, ester.velazquez@urjc.es, hodei.urrutxua@urjc.es, pablo.solano@urjc.es

***Abstract* – This work addresses the optimal design of berthing missions with non-cooperative Resident Space Objects. In particular, a recently introduced general optimal control solver is revisited from both the theoretical, practical and computational perspective. While originally constructed upon collocation and shape-based methods, connections to modern Pseudospectral Theory are outlined. Comparison against standard optimal control techniques is also achieved to demonstrate its performance, advantages, and flaws. Once done, the solver is applied to the integral trajectory optimization of berthing missions: from low-thrusted rototraslational rendezvous to the deployment and pre-capture phase of the target via a robotic arm. A complete guidance and control architecture is then constructed upon this optimization engine by embedding it within a Model Predictive Control, Real-Time Iteration scheme. Both Model and Hardware in the Loop campaigns (at the rendezvous laboratory of the University Rey Juan Carlos) are introduced to verify and validate the system for real-time, embedded GNC applications, while highlighting the intrinsic synergies between its building blocks.**

I. INTRODUCTION

The exponential increase of human activities in space is leading to a major congestion of the near-Earth regime, thus becoming a major threat to the sustainable use of the space environment. In this scenario, Active Debris Removal (ADR) missions have become a necessary enabling concept in order to avoid the well-known Kessler syndrome [1]. Among options [2] robotics for in-space capture and passivation of Resident Space Objects (RSO) has recently appeared as an ever-green field of research on which this communication is focused. Indeed, since the early days of the Space Era, robotics have played a fundamental role in the development of space missions of all kinds, especially blooming since the mid-1990s [3].

Robotic missions are characterised by tight performance constraints, which normally translate into formal Optimal Control Problems (OCP) for the mission design engineer. In fact, control-state trajectory optimization is a central challenge in not only robotic, but in all space exploration activities. In spite of the vast literature on the topic, Optimal Control still poses untackled problematics, especially with regards to Real Time Optimal Control onboard legacy systems [4]. The solutioning process behind OCP is constrained by the need to solve complex Nonlinear Programming Problems (NLP) associated to a Hamiltonian Minimization Condition (HMC), such as Pontryagin's Minimum Principle (PMP). This challenge particularly applies to short-time scales (high-frequency) applications, such as berthing and proximity operations with non-cooperative, tumbling targets, as required by ADR activities [5].

The application of robotic manipulators to berthing missions have been long studied in the literature, while in a particular niche fashion. Usually, efforts are focused on the optimal planning of the robot trajectory, while the complete mission design is not covered [6] or vice versa. Moghaddam and Chhabra provides a thorough, comprehensive review of the main technical challenges and techniques of robotic space missions from a GNC and optimal control perspective [7]. Path planning studies date back to the 1990s, when global optimization techniques for redundant end-effectors were investigated by Agrawal and Xu [8]. Papadopoulos and Abu-Abed investigated motion planning for zero-reaction manipulators [9]. In [10], authors already investigated optimal motion planning for free-flying robots in their joint space, in the absence of spacecraft actuation, through shape-based methods and Sequential Quadratic Programming (SQP). Both the optimal pre-capture and passivation of tumbling RSO with unknown dynamics by means of PMP were studied by Aghili, where simulations on real robotic hardware were also presented [11,12]. Boyarko et al., in a series of works, combined pseudospectral methods and inverse dynamics for the very same problem, including analysis on the real-time deployment of their OCP solving technique [13,14]. Similarly, Michael et al. applied numerical collocation to both the modelling and optimal path planning for ADR missions [15]. Relevant for this investigation again, Wilde et al. researched on experimental characterization of docking with a tumbling RSO through inverse dynamics and polynomial-based prescription of the robot state [16] similarly to Caubet and Biggs [17], Stoneman and Lampariello [18] or Ventura et al. [19] More recently, Virgili-Llop et al. have addressed the optimal deployment of robotic arms for proximity operations missions through Sequential Convex Programming (SCP) [20]. In [21], Flores-Abad et al. designed a two-step method to determine both the optimal capture time

and the rendezvous trajectory to a tumbling object, which numerically relied again on pseudospectral methods. Stenberg elaborated on the study of optimal docking to tumbling object in the presence of uncertainty [22], a situation commonly encountered in ADR missions. The feasibility of proximity operations with tumbling RSO by means of reachable sets, based on minimum time optimization, has been elaborated by Zagaris [23]. Xu et al. have investigated in a recent work optimal guidance for docking with tumbling spacecraft by means of PMP directly, including also collision avoidance policies [24]. Finally, modern control techniques have also led their way into the problem, as demonstrated by the use of Sliding Mode Control in Abdollahzadeh and Esmailifar [25] or robust tube-based MPC in Dong et al. [26], or Specht and Lampariello [27, 28]; the latter also discussed real-time applications of the proposed algorithm. Along this line, Santos, Rade and Fonseca have introduced machine learning strategies to solve optimal path planning of robotic manipulators [29]. Zhang et al. have just analysed the capture of tumbling objects using again pseudospectral collocation, but in combination with reinforcement learning [30]. Abundant literature may also be found addressing the optimal design of the rendezvous phases of the mission, from the long-range phase to the sub-meter approximation to the RSO. Modern enabling control techniques, such as Model Predictive Control and Convex Optimization, may also be found at the core of such studies, showing now a consolidated background for rendezvous applications [31-42]. Precisely, this is the focus of the recent work by Rebollo et al. [43], for example, and the references therein among others.

Compared to previous literature, this communication presents an integral and optimal design of berthing space mission with non-cooperative RSO. In particular, interest is given not only to the deployment of a robotic arm actuator during the pre-capture process, but also to the optimal 6 DoF rendezvous trajectory design with the target RSO in an arbitrary elliptic orbit. The differential flatness properties of the rendezvous low-thrust Tschauner-Hempel model [44] and the convex, hybrid kinematics of Modified Rodrigues Parameters [45] are exploited for cost-effective solutioning of the associated open-loop trajectory OCP. As the inner guidance engine, we revisit a novel optimal control solver of generic purpose, introduced in [46]. The solver is characterized by a cost-effective design, based on orthogonal collocation and shape-based techniques. Once presented, connections to Pseudospectral Theory are established, and its performance validated against standard OCP solving techniques (SCP) to verify its effectiveness. Furthermore, in order to construct a complete guidance and control loop, the algorithm is deployed as an optimal trajectory planner within an outer Model Predictive Control loop. Finally, the performance of the design is verified and validated in two-fold. On the one hand, close-loop trajectory optimization of berthing missions is presented in Model in the Loop simulations. Second, Hardware in the Loop campaigns are executed to deploy the complete guidance and control architecture onto realistic mission scenarios missions in the Space Proximity Operations Laboratory (SPOL) at University Rey Juan Carlos; wit the aim of demonstrating the algorithm in the design of optimal berthing trajectories to non-cooperative, tumbling targets, implemented onboard a 6 DoF robotic arm. This communication builds on and extends the results in Cuevas et al. [47], which, in comparison, focused on open-loop optimization only.

The remainder of this communication is divided as follows. Section II reviews the novel optimal control solver proposed, including both theoretical, and computational insights, and its numerical demonstration on classical OCP examples. Moreover, similarities and differences with state-of-the-art techniques are highlighted. Section III develops general berthing mission phases as OCP through the introduction of the aforementioned differentially-flat models, as required by the guidance algorithm. However, for real-time applications and to manage uncertainties, Section IV presents a Nonlinear Model Predictive (NMPC) architecture within which the optimization engine is embedded. In Section V practical numerical demonstrations of the above techniques are introduced, and the performance of the solver strictly analysed. Finally, the results of a Hardware in the Loop campaign are presented in Section VI, together with a brief discussion of the overall rendezvous setup. Concluding remarks, steps ahead and open lines of research are discussed in Section VII.

II. COST-EFFECTIVE GUIDANCE THROUGH SBOPT

The resolution of OCP is primarily coped with numerical techniques, as in only few cases, analytical or close-form solutions are available. This is even more relevant for autonomous missions, such as berthing ones. This Section explores the numerical solver used in this work to handle all OCP homogeneously.

As already introduced, the design of an optimal control law is constrained by the need to solve a HMC [48] Traditional approaches to the solution of this HMC relies on the classical indirect and direct methods [49], which either solve the primal-dual problem or rely on discretization or collocation for solving a finite NLP. However, the introduction of the pseudospectral (PS) family of solvers in the early 2000s has led to a change of paradigm. PS solvers show both theoretical and numerical advantages for practical optimal control onboard digital computers [50]. Remarkably, they have

recently blurred the barrier between direct and indirect methods, manifesting their equivalency [51], and have initiated the field of Hamiltonian Programming, in comparison to NLP, which addresses the formal mathematical structure of OCP [51-53]. Although several formulations of PS methods exist [54-56] all of them employ direct collocation of the state-control pair on the nodes of a family of orthogonal polynomials and associated Gaussian quadratures. See [4] for a detailed review of these techniques.

Instead of leveraging classical Optimal Control software, we resort into an in-house, high-efficient algorithm and cost-effective numerical solver for OCP, SBOPT, which was presented in Solano et al. [46] and further reviewed in Cuevas et al. [47]. SBOPT builds on the recent work of the astrodynamics community on shape-based solvers [57-64]. The latter are characterized by projecting the state evolution of the system on pre-selected functional families, leading to small optimization problems on the parameters spanning such families. Compared to classical direct or indirect methodologies, shape-based techniques allow for a quick generation of boundary-compliant initial guesses for optimization solvers (notably, for direct transcription ones) as long as the selected functional base is able to capture the problem's intrinsic dynamical features.

While SBOPT was initially planned as another general shape-based solver, it soon showed analogies and theoretical fundings rooted in classical PS theory (starting from its object-oriented user interface, inspired by DIDO [52]). This special architecture of the solver hybridizing shape-based and PS methods provides a cost-efficient technique, suited for embedded applications. In terms of performance, it compares to convex optimization schemes, as demonstrated in the examples. Nonetheless, at its current stage, both convergence, feasibility and accuracy proofs are still to be constructed. The technique is now briefly sketched for completeness purposes. Again, a complete overview of the method may be found in [47].

The objective of SBOPT is to accurately and efficiently solve realizations of the following general optimal control problem

$$\begin{aligned} \min J = {} & M\big(\mathbf{x}(t_0), \mathbf{x}\big(t_f\big), t_0, t_f\big) \\ & + \int_{t_0}^{t_f} l(\mathbf{x}(t), \mathbf{u}(t), t)\ \mathrm{d}t, \\ s.t. \quad & \boldsymbol{f}(\boldsymbol{\mu}, t, \mathbf{x}, \mathbf{x}^k) + \boldsymbol{g}(\boldsymbol{\mu}, t, \mathbf{x}, \mathbf{x}^k, \mathbf{u}) = \mathbf{0}, \\ & \boldsymbol{e}_0\big(t_0, \mathbf{x}(t_0)\big) = \mathbf{0}, \\ & \boldsymbol{e}_f\left(t_f, \mathbf{x}\big(t_f\big)\right) = \mathbf{0}, \\ & \boldsymbol{h}(\boldsymbol{\mu}, t, \mathbf{x}, \mathbf{u}) \leq \mathbf{0}, \end{aligned} \tag{1}$$

where the state of the dynamical system is described by the vector $\mathbf{x}$ and its k-th derivative $\mathbf{x}^k$, and whose evolution with respect to the independent variable t is governed by the vector fields $\boldsymbol{f}$ and $\boldsymbol{g}$, characterized by a set of parameters $\boldsymbol{\mu}$ and the control vector field $\mathbf{u}$. Mixed control-state path constraints are encoded within the function $\boldsymbol{h}$, while $\boldsymbol{e}_i$ enforce boundary conditions on $\mathbf{x}$ through generally nonlinear maps.

The fundamental feature of the method is the use of pre-determined functional bases to describe the optimal solution, thus showing similarities with the classical shape-based solvers. In our method, the configuration (not the state) vector $\mathbf{s} \in \mathbb{R}^{N_s}$ is projected onto some polynomial basis $\wp$ parametrized by the polynomial time τ.

$$\mathrm{s}_i(\tau) = \sum_{j=0}^{p_i+1} c_{ij}\, P_j(\tau)\,, i = 1,2,..,N_s. \tag{2}$$

The polynomial order set $\mathbb{N} = \{p_i\}_{i=0}^{N_s}$ defines the order of the expansion of each of the configuration vector components. In matrix notation, the above can be compactly written as a linear application

$$\begin{gathered} \mathbf{s}(\tau) = CP(\tau) \in S[\tau], \qquad P \in \mathbb{R}^{N+1} \times \mathbb{R}, \\ C = [\boldsymbol{c}_0, \boldsymbol{c}_1, \dots, \boldsymbol{c}_N, \boldsymbol{c}_{N+1}] \in \mathbb{R}^{N_s \times N+1}. \end{gathered}$$

Here $S[\tau]$ denotes the polynomial ring in τ and N is the maximum present polynomial order in $\mathbb{N}$. Moreover, it is clear than from (2), all state derivatives are readily available by differentiation of polynomials, so that the problem's dependency on them is explicitly avoided for the ease of notation, $\mathbf{x} = \boldsymbol{t}(\mathbf{s})$. As it will become apparent, the ultimate goal of the methodology here proposed is the optimization of C to represent an extremal solution to Problem (1).

The transcription of the Bolza functional problem is achieved by means of collocation onto a Gaussian quadrature over the polynomial time τ, defined by a finite set of collocation points $\mathrm{T} = \{\tau_i\}_{i=0}^{m}$. The set T is ordered so that τ_i is monotonically increasing. When applicable, this discretization defining the quadrature is selected to match the nodes of the polynomial basis selected, as in PS methods: for Legendre polynomials, the Legendre-Gauss-Lobatto (LGL) quadrature is used [65]; Clenshaw-Curtis quadrature follows for Chebyshev polynomials [66]. For finite-horizon problems ($t_f - t_0 \in \mathbb{R}$), the polynomial time interval $\tau \in \Im$ shall be closed, to allow to strictly imposed boundary conditions at τ_0 and τ_m. Moreover, to handle homogeneously both time fixed and time-free problems, the nondimensional time is introduced

$$\theta = \frac{t - t_0}{t_f - t_0} \in [0,1],$$

so that the following holds

$$t_i = \left(t_f - t_0\right)\theta_i = \left(t_f - t_0\right)\sigma_i(\tau_i), i = 0, 1, \dots, m.$$

The number of nodes m can be independently selected from the polynomial approximation order N. Usually, some heuristic is used to link the two. The use of general quadratures usually provides upper bounds of m as a function N of for accurate numerical integration (Gauss quadrature is exact for polynomials of order $N < 2m - 1$, for example). For a Cauchy TBVP, a minimum third-order polynomial expansion is needed to allow free degrees of freedom to be determined.

The collocation grid / quadrature T allows to trivially evaluate the original cost functional J

$$J \approx M\left(\mathbf{s}(\tau_m), \mathbf{s}(\tau_0), t_f, t_0\right) + \\ +\left(t_f - t_0\right)\sum_{i=0}^{m} w_i\, l(\mathbf{s}(t_i), \mathbf{u}(t_i), t_i)\, \mathrm{d}\sigma_i.$$

In the above, w_i defines the quadrature weights associated to each of the collocation points τ_i. Given that, in general, the physical time $\mathfrak{I} \neq [t_0, t_f]$ shall be evaluated as a function of the points τ_i through the nonlinear map σ, the quadrature shall be scaled by its differential $\mathrm{d}\sigma_i$.

The imposition of the dynamic constraints is intrinsically achieved by computing the control law $\mathbf{u}$ as a residual of the differential form of the dynamics, similarly to differential inclusions [67] or dynamics inversion [68], with differentially flat systems as the maximal expression of the latter [69,70]. SBOPT directly works in the tangent space of the dynamics. This approach avoids the need of any implicit integration, compared to classical direct methods [71], as it imposes the dynamic constraints, the crux of all direct methods [67], in differential, rather than integral form. In short, the control law $\mathbf{u}$ evaluated at the discrete grid T can be computed as the solution to

$$\mathbf{u}(\tau_i) : \boldsymbol{f}(\mu, t_i, \mathbf{s}_i) + \boldsymbol{g}(\mu, t_i, \mathbf{s}_i, \mathbf{u}_i) = \mathbf{0}.$$

In this way, when compared to traditional direct collocation schemes (including PS methods), the control signal $\mathbf{u}$ is not part of the decision variables to be optimized, but it is just computed as a byproduct of the geometrical optimization of the configuration vector $\mathbf{s}$. This results in a major reduction of the computational needs of the problem.

Additionally, in our approach, the inclusion of the boundary conditions is explicitly achieved by prescribing the functional/polynomial shape of the trajectory. In this way, the optimization solver only needs to handle path constraints. This is achieved by defining the symmetric set $\mathcal{B} = \{\boldsymbol{c}_0, \boldsymbol{c}_1, \boldsymbol{c}_N, \boldsymbol{c}_{N+1}\}$ of polynomial coefficients and then fixing it to satisfy the boundary conditions at each iteration of the optimization, through an appropriate linear system of equations in close form.

$$\sum_{\boldsymbol{c}\in\mathcal{B}} \boldsymbol{c}_j\, P_j(\tau_i) = \mathbf{s}_i - \sum_{\boldsymbol{c}\notin\mathcal{B}} \boldsymbol{c}_j\, P_j(\tau_i), \qquad i = 0, f.$$

All in all, the decision variable set to be optimized within the solver is therefore reduced to $\boldsymbol{Z} = \left[\left\{\boldsymbol{c}_j^{\mathrm{T}}\right\}_{\boldsymbol{c}_j\notin\mathcal{B}}, t_0, t_f, \boldsymbol{\beta}^T\right]^{\mathrm{T}}$, where $\boldsymbol{\beta}$ includes any additional degree of freedom or parameter of the problem.

For a given TBVP problem of Bolza of the form of. (1), the final transcripted version is now the following geometrical problem

$$\min_{\boldsymbol{Z}} J = M\left(\mathbf{s}(\tau_m), \mathbf{s}(\tau_0), t_f, t_0\right) + \\ +\left(t_f - t_0\right)\sum_{i=0}^{m} w_i\, l(\mathbf{s}(t_i), \mathbf{u}(t_i), t_i)\, \mathrm{d}\sigma_i,$$

$$s.t \quad \begin{aligned} &\boldsymbol{e}_0\left(t_0, \mathbf{s}(t_0)\right) = \mathbf{0}, \\ &\boldsymbol{e}_f\left(t_f, \mathbf{s}(t_f)\right) = \mathbf{0}, \\ &\boldsymbol{h}(\boldsymbol{\mu}, t_i, \mathbf{s}_\mathrm{i}, \mathbf{u}_\mathrm{i}) \leq \mathbf{0}. \end{aligned} \qquad (3)$$

Standard NLP solver algorithms suffice to compute the solution of problem (3), without the need of accurate initial guesses $\boldsymbol{Z}_0$ (which can be easily nonetheless provided to speed up convergence). In this paper, these are generated by simply collocating a 3rd order spline to satisfy the boundary conditions and over-sampling it to generate C_0 [63]. Moreover, all examples have been computed using SQP, as built in Matlab's fmincon function [72,73].

In summary, the proposed methodology shares common features with PS methods (collocation in differential form, use of orthogonal polynomials as main representations of the state) but they fundamental differ in the following:

- The state is represented in modal versus nodal form in standard PS algorithms: the polynomial coefficients become the main optimization variables, instead of optimizing sampled snapshots of the state evolution. This leads to usually smaller optimization problems in terms of memory and cost.
- Moreover, such representation only affects the configuration vector instead of the state one, allowing to handle systems in its direct differential order form (Newton's Laws

versus first-order state space representations). Again, this impacts the memory requirements of the process [74].

- Differentiation is not performed by means of spectral matrices, but directly through analytic computation of the derivative of the basis during the setup of the method. The avoidance of such differentiation matrices leads to numerically better conditioned collocation for dense grids, as opposed to standard PS cases [75]. In particular, SBOPT is an inexact realization of the computationally advantageous Birkhoff PS methods [76,77], aiming to constitute an example of HMP in the near future.
- The control signal **u** is not an optimization variable. Instead, it is computed by means of the dynamics inversion principle, leading to pure problems from calculus of variations. While this comes with additional flaws, as seen next, it also avoids the need to interpolation in order to implement the control law in real time. Indeed, it leads to close-form, analytical expressions of the optimal control solution.

Before introducing the design of berthing missions, three simple OCP examples are discussed quantitatively to expose the virtues and drawbacks of SBOPT and compare its performance against sequential convex programming (as a state-of-the-art numerical OCP solving technique).

Quadratic optimization is the workhorse in space optimization, given the availability of close-form (sometimes analytical) solutions, among which Kalman's Linear Quadratic Regulator (LQR) stands out. Naturally, the LQR will provide our first opportunity to demonstrate the capabilities of the solver. Consider the following 1D OCP

$$\begin{aligned} \min J &= \frac{1}{2}\int_{t_0}^{t_f} \mathrm{u}^2 \ \mathrm{d}t, \\ s.t. \quad \ddot{\mathrm{s}} &= \mathrm{u}, \\ (\mathrm{s}_0, \dot{\mathrm{s}}_0) &= \mathbf{0}, \\ (\mathrm{s}_f, \dot{\mathrm{s}}_f) &= (1,0), \\ t_0 = 0, t_f &= 1. \end{aligned}$$

The application of PMP leads to the following optimal control law

$$\mathrm{u}^* = -12t + 6, \qquad \mathrm{s}^* = -2t^3 + 3t^2;$$

which, as seen in the following Fig. 1 and 2, is perfectly reproduced by SBOPT.

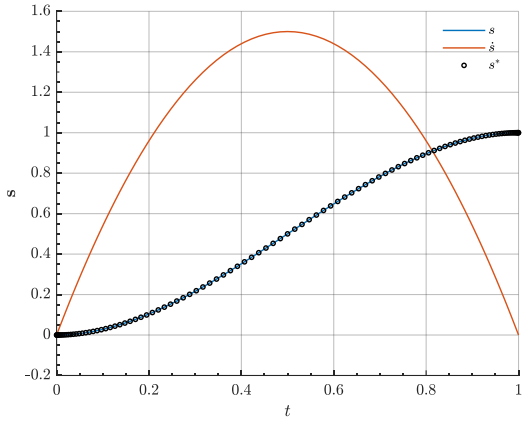

Figure 1. SBOPT and analytical solution of the 1D LQR problem (state).

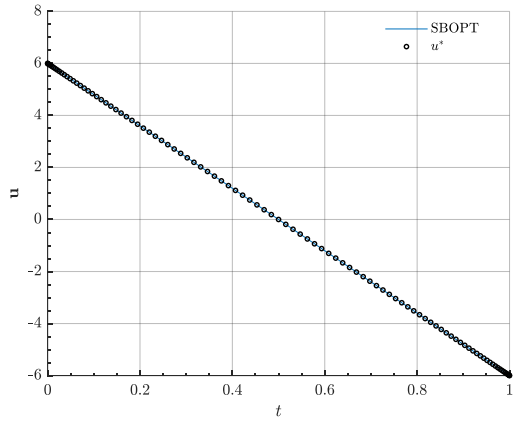

Figure 2. SBOPT and analytical solution of the 1D LQR problem (control).

Consider now the classical Breakwell's problem [48] (a state-constrained LQR), whose statement reads

$$\begin{aligned} \min J &= \frac{1}{2}\int_{t_0}^{t_f} \mathrm{u}^2 \ \mathrm{d}t, \\ s.t. \quad \ddot{\mathrm{s}} &= \mathrm{u}, \\ (\mathrm{s}_0, \dot{\mathrm{s}}_0) &= \mathbf{0}, \\ (\mathrm{s}_f, \dot{\mathrm{s}}_f) &= (1,0), \\ \mathrm{s} &\leq l, \\ t_0 = 0, t_f &= 1. \end{aligned}$$

In the above, $l > 0$ is a parameter of the system. When solved numerically via SBOPT (for $N = 10$ and $m = 100$, using LGL quadrature, in less than 0.11s), the results are able to capture the discontinuous nature of the optimal control law, as seen in Fig. 3 and 4. However, Gibbs' phenomenon is present in the solution. In short, the solver implicitly assumes a level of regularity of the control application which is in this case not in agreement with the true solution. Such effect roots in the fact that the control is computed as a residual, and therefore inherits the polynomial nature of the operations in the

dynamics function: in this case, given that $\mathbf{s}$ is prescribed to be polynomial and differentiation is a polynomial operation, the control is forced to be polynomial also. For the general optimal control problem, however, this is not the case (technically, the common assumption is $\mathbf{s} \in W^{1,1}$, but $\mathbf{u} \in L^{\infty}$; the solver here assumed $\mathbf{u} \in W^{1,1}$). Traditional PS methods avoid such nuance by resorting into the nodal representation of the state-control pair (discrete evaluation over the independent variable) [48] versus our more compact modal representation of the solution.

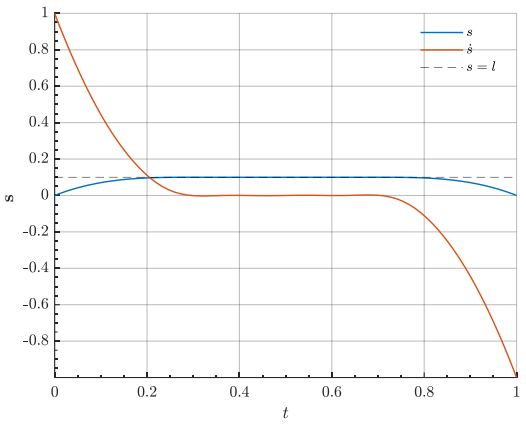

Figure 3. SBOPT and analytical solution to Breakwell's problem (state).

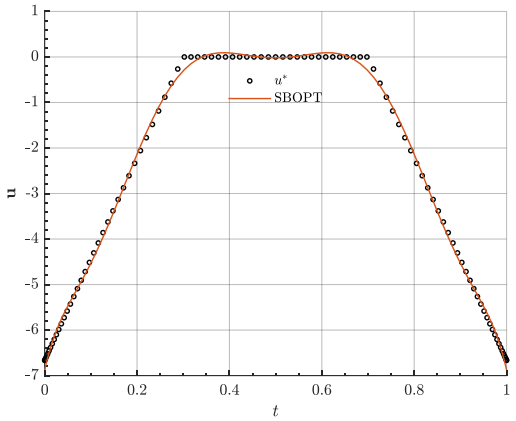

Figure 4. SBOPT and analytical solution of Breakwell's problem (control).

Finally, SBOPT will now be compared against standard OCP solving techniques, to demonstrate its capabilities. In particular, the following attitude slewing problem in Modified Rodrigues Parameters (MPR) is conceived.

$$
\begin{aligned}
&\min J = \frac{1}{2}\int_{t_0}^{t_f} \mathbf{u}^{\mathbf{T}}\mathbf{u}\ \mathrm{d}t,\\
s.t.\quad &\dot{\boldsymbol{\sigma}} = \frac{1}{4}B(\boldsymbol{\sigma})\boldsymbol{\omega},\\
&I\boldsymbol{\omega} + \boldsymbol{\omega}\times I\boldsymbol{\omega} = \mathbf{u},\\
&\dot{\boldsymbol{h}} + \boldsymbol{\omega}\times\boldsymbol{h} = -\mathbf{u},\\
&||\boldsymbol{\omega}(t)||_{\infty} \le \omega_{\max},\\
&||\boldsymbol{h}(t)||_{\infty} \le h_{\max},\\
&||\mathbf{u}(t)||_{2} \le \mathrm{u}_{\max},\\
&||\boldsymbol{\sigma}(t)||_{2} \le 1,\\
&(\boldsymbol{\sigma}_{\mathbf{0}}, \boldsymbol{\omega}_0, \boldsymbol{h}_0) = \mathbf{0},\\
&(\boldsymbol{\sigma}_{\mathbf{0}}, \boldsymbol{\omega}_0, \boldsymbol{h}_0) = (1,0,0,\mathbf{0}),\\
&t_0 = 0, t_f = t_f^{\max}.
\end{aligned}
$$

For brevity, we do not go into describing the derivation and formalities of this formulation. The nonlinear nature of the kinematic-dynamic equations requires of Sequential Convex Programming (SCP) to solve the problem. Nonetheless, when linearized, the above can be posed as a Second Order Cone Programming Problem (SOCP), which can be efficiently solved by available numerical techniques, such as through ECOS (an embbedable, user-friendly, and lightweight algorithm capable of handling general SOCP [78]). To solve the problem, discretization/collocation is needed. In this case, classical Lagrange PS theory will be used to provide the finite NLP problem to be solved.

The results obtained for the same, arbitrary problem by this architecture (SCP via ECOS and the techniques outlined in [79,80]) are compared against those of SBOPT in the following Table 1. Fig. 5 and 6 depict the state evolution and relevant variables of the problem. Remarkably, despite showing similar results for the optimal cost value, the difference in the computational cost (measured on the same machine) allows to quantitively compare SBOPT to these state-of-the-art methods in OCP (a truly objective conclusion would deserve a discussion on its own right on the numerical implementation of both techniques).

Table 1. Results comparison between ECOS-PS and SBOPT for a generic attitude slew problem.

	SCP-ECOS-PS	SBOPT
N	N/A	7
m	50	50
Optimal cost	1.47E-8	5.45E-09
Comp. cost [s]	27.67	1.42

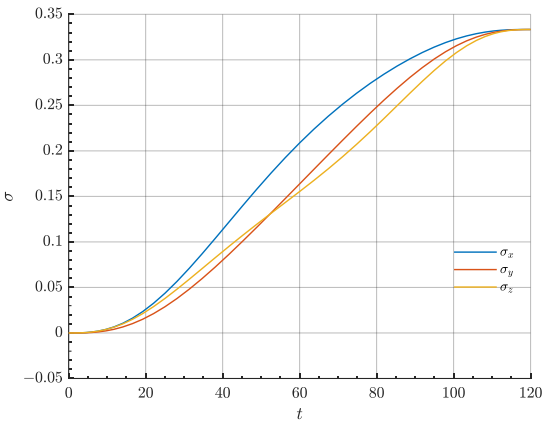

Figure 5. Predicted open-loop MRP trajectory.

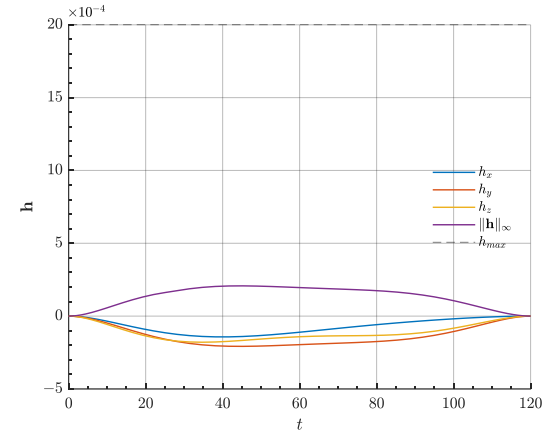

Figure 6. Predicted open-loop angular momentum trajectory (reaction wheel actuators).

III. Flat Integral Berthing

This Section present the different modelling techniques used to provide a computationally feasible OCP, to be solved in real time through SBOPT. Because of the solver, specific differentially flat models are used. These will be referred as GNC models, in comparison to the ones used in simulations.

Consider a general nonlinear system

$$\dot{\mathbf{x}} = \boldsymbol{f}(\mathbf{x}, \mathbf{u}),$$

where $\mathbf{x}$ is taken to live in an appropriate n dimensional state space and $\mathbf{u}$ is the control input. The system is defined to be flat if there exists an m dimensional state vector $\boldsymbol{\chi}$ of differentially independent components such that [81]

$$\boldsymbol{\chi} = \boldsymbol{\varphi}(\mathbf{x}, \mathbf{u}, \dot{\mathbf{u}}, \dots, \mathbf{u}^k), \qquad \begin{cases} \mathbf{x} = \boldsymbol{\phi}_{\mathrm{x}}(\boldsymbol{\chi}, \dot{\boldsymbol{\chi}}, \dots, \boldsymbol{\chi}^k) \\ \mathbf{u} = \boldsymbol{\phi}_{\mathrm{u}}(\boldsymbol{\chi}, \dot{\boldsymbol{\chi}}, \dots, \boldsymbol{\chi}^k) \end{cases},$$

The elements of $\boldsymbol{\chi}$ are known as flat outputs. See [82] for in-depth technical details of flat systems. For linear systems, differential flatness implies controllability and vice versa [82].

Flat systems are interesting for onboard optimal guidance, as they allow to restrict the formulation of OCP to a pure geometrical optimization within the realm of the calculus of variations. In particular, they set a generic Bolza problem into a (much more reduced) problem of the form

$$\min J(\boldsymbol{\chi}), s.t \quad \boldsymbol{h}(\boldsymbol{\mu}, t, \boldsymbol{\chi}) \leq \mathbf{0}. \tag{4}$$

When cast into a finite dimensional problem (by means of discretization or collocation), the above results into a suitable NLP, usually much simpler than its in original Bolza statement. Moreover, if the problem enjoys additional properties (convexity), (4) can be solved by efficient means.

Berthing missions with uncooperative, passive targets require of both the translational and rotational path planning of the chaser to allow the capture of the former. As a result, both the relative orbital motion and attitude kinematics and dynamics shall be studied by appropriate models.

While linear models in rendezvous scenarios are supported by the nature of the mission itself (approaching the target), berthing in arbitrary elliptic orbits discards the celebrated Hill-Clohessy-Wiltshire model [83] as a valid modelling approach. Instead, in this work the more general, anomaly-dependent Tschauner-Hempel model (TH) is leveraged [44]. Moreover, it benefits from flat properties [81]. Denote by $\mathbf{r}_t$ the target position vector, realised in a suitable Local Vertical Local Horizontal (LVLH) reference frame defined by

$$\boldsymbol{k} = -\frac{\mathbf{r}_t}{\mathrm{r}_t}, \qquad \boldsymbol{j} = -\frac{\mathbf{r}_t \times \dot{\mathbf{r}}_t}{||\mathbf{r}_t \times \dot{\mathbf{r}}_t||}, \qquad \boldsymbol{i} = \boldsymbol{j} \times \boldsymbol{k}.$$

Let $\boldsymbol{\rho} = [x, y, z]^{\mathbf{T}}$ be the relative position vector of the chaser with respect to the target, in the LVLH frame. Introduce the transformation parameter k

$$k(\theta) = 1 + e \cos\theta,$$

where e is the osculating target orbit eccentricity and θ is the corresponding true anomaly, which replaces time as the independent variable. Equally, let $n = \mu/h^{3/2}$ be the target's orbit mean motion. In arbitrarily canonical units ($\mu = 1$), the relative dynamics of the chaser are driven by

$$\begin{cases} x'' = 2z' + \dfrac{1}{n^2k^3}u_x \\ y'' = -y + \dfrac{1}{n^2k^3}u_y \\ z'' = \dfrac{3}{k}z - 2x' + \dfrac{1}{n^2k^3}u_z \end{cases}$$

The TH model provides the control flow of 3 out of the 6 DoF of the chaser as a rigid body. The remaining 3 correspond to the rotational dynamics of the problem (which will also include those of the target).

Define a body reference frame B_i as a dexteral triad of versors $\{\boldsymbol{i}_i, \boldsymbol{j}_i, \boldsymbol{k}_i\}$ attached to the center of mass of either the target or the chaser. The evolution of the angular velocity $\boldsymbol{\omega_i}$ between the body and inertial frames, realised in the former, is dictated by the Euler-Poinsot Initial Value Problem (IVP) system

$$I\dot{\boldsymbol{\omega}}_\iota + \boldsymbol{\omega}_i \times I\,\boldsymbol{\omega}_i = \boldsymbol{\tau},\ \boldsymbol{\omega}_i(t_0) = \boldsymbol{\omega}_i^0 \qquad (5)$$

in which I is the associated inertia matrix in the body frame. Typically, the inertia of the target will not be accurately known but shall be observed online. This work assumes an observability condition on I. Here, $\boldsymbol{\tau}$ denotes the control input of the system, i.e., the applied torque. Because the target is passive, it is clear that $\boldsymbol{\tau} = \mathbf{0}$, thus undergoing free-torque motion (abundant literature approaches the target capture phase by aligning the docking fixture of the chaser with the invariant spinning axis of the target).

Once the evolution of the body frame angular velocity is known (or predicted), the attitude kinematics between the body frame and an arbitrary reference system can be studied, by means of the following IVP

$$\dot{\boldsymbol{\sigma}}_J = \frac{1}{4}B(\boldsymbol{\sigma})\boldsymbol{\omega}_j, \qquad \boldsymbol{\sigma}_i(t_0) = \boldsymbol{\sigma}_i^0.$$

The Modified Rodrigues Parameters (MRP) $\boldsymbol{\sigma}$, the stereographic projection of the attitude configuration manifold S^3 [45], are used to parametrize the attitude kinematics because they can be demonstrated to be flat [84] Matrix B is a quadratic form on $\boldsymbol{\sigma}$, see [84] for details. In the above, $\boldsymbol{\omega}_j$ represents the angular velocity between the body frame and the arbitrary selected one, and $\boldsymbol{\sigma}$ transforms vector realisations from the later to the former. The use of MRP comes with additional flavours: when compared to other typical covers of S^3, such as quaternions, these lead to convex non-holonomic geometric constraints

$$||\boldsymbol{\sigma}(t)|| \leq 1,$$

which are computationally preferred over other options (such as the classical unit quaternion constraint). If the shadow set $\boldsymbol{\sigma}^S$ is introduced,

$$\boldsymbol{\sigma}^S(t) = -\frac{\boldsymbol{\sigma}}{\boldsymbol{\sigma}^{\mathrm{T}}\boldsymbol{\sigma}},$$

the MRP become a non-singular double-cover of S^3. For both the regular and shadow MRP, the attitude kinematics remain the same. Because SBOPT works directly on the tangent space of the trajectory, this is computationally advantageous, because the non-holonomic constraint can be replaced through a trivial normalization operation in the kinematics vector field.

Precisely, the flat outputs of the system are $\boldsymbol{\sigma}$. When exploited, this leads to the following flat form of the attitude problem.

$$\begin{cases} \boldsymbol{\omega}_j = 4\,B^T(\boldsymbol{\sigma})\dfrac{\dot{\boldsymbol{\sigma}}}{(1+\boldsymbol{\sigma}^T\boldsymbol{\sigma})^2} \\ \boldsymbol{\tau} = \boldsymbol{\omega}_j \times I\,\boldsymbol{\omega}_j + \dfrac{4}{(1+\boldsymbol{\sigma}^T\boldsymbol{\sigma})^2}\ B^T(\boldsymbol{\sigma})\left[\ddot{\boldsymbol{\sigma}} - \dfrac{1}{4}\dot{B}(\boldsymbol{\sigma})\boldsymbol{\omega}_j\right] \end{cases}$$

To complete the IVP, initial conditions shall be expressed as the initial values for both the MRP and its first-order derivative. This can always be accomplished by mapping the physical angular velocity $\boldsymbol{\omega}_0$ to $\dot{\boldsymbol{\sigma}}_0$ through the attitude kinematics field.

In fact, the attitude problem will be studied with respect to the LVLH frame, which introduces inertial terms into (5), corresponding to restricting the evolution of $\boldsymbol{\omega}$ to be that of the body frame with respect to the LVLH (both being not inertial). These are not contemplated in SBOPT but hold in the high-fidelity simulations for the MIL campaign.

We are now able to pose the berthing OCP problem as the following coupled, geometrical optimization

$$\begin{gathered} \min J = \int_{t_0}^{t_{\max}} \mathbf{u}^{\mathrm{T}}\mathbf{u} + \boldsymbol{\tau}^{\mathrm{T}}\boldsymbol{\tau}\ \mathrm{d}t, \\ s.t. \quad [\mathbf{u}^{\boldsymbol{T}}, \boldsymbol{\tau}^{\boldsymbol{T}}]^{\boldsymbol{T}} = \boldsymbol{f}(n, e, \theta, h, I, \mathbf{s}), \\ \mathbf{s}(t_0) = \mathbf{s}^0, \\ ||\dot{\boldsymbol{\rho}}||_\infty \leq v_{\max}, \\ ||\boldsymbol{\omega}||_\infty \leq \omega_{\max}, \\ ||\mathbf{u}||_2 \leq \mathrm{u}_{\max}, \\ ||\boldsymbol{\tau}||_\infty \leq \mathrm{u}_{\max}, \\ ||\boldsymbol{g}(\delta\boldsymbol{\sigma}_t)\boldsymbol{\omega}_{\boldsymbol{c}}(t_{\max}) - \boldsymbol{\omega}_t(t_{\max})||_\infty \leq \epsilon_\omega, \\ A\boldsymbol{g}(\delta\boldsymbol{\sigma}_t)\boldsymbol{\rho} \leq c, \\ -\boldsymbol{g}(\delta\boldsymbol{\sigma}_t)\boldsymbol{d}_c^T\boldsymbol{d}_t \geq \cos\theta_a, \\ \boldsymbol{\rho}^T\boldsymbol{\rho} \leq L_g. \end{gathered} \qquad (6)$$

The dynamics constraints $\boldsymbol{f}$, following they are flat, are interpreted as the way to compute the control vectors $[\boldsymbol{u}^{\boldsymbol{T}}, \boldsymbol{\tau}^{\boldsymbol{T}}]^{\boldsymbol{T}}$. Here $\mathbf{s}$ is the flat output of the system**.** The relative attitude between the chaser and the target is characterized by the relative MRP $\delta\boldsymbol{\sigma}_t$.

The problem constraints correspond to saturation of both the angular and linear velocity of the chaser, as well as bounds on its control authority. Moreover, a LOS corridor constraint (through the convex inequality $\{A, c\}$) is enforced, together with a requirement of alignment between the grasping fixtures of the chaser and target, $\boldsymbol{d}_c$ and $\boldsymbol{d}_t$ (realised in their respective body frames). Note that the boundary conditions at the final epoch are open (while fixed at t_0), but restricted through the above LOS and alignment constraints, together with the need of ending the manoeuvre within a sphere of radius L_g centred at the target (corresponding to the maximum reachability of the robotic arm to be deployed). Finally, at the end epoch, the angular velocity of both vehicles shall match up to a tolerance of ϵ_ω. Note that the attitude problem requires of appropriate transformations to be expressed as a function of the target's true anomaly, as required by the TH model. Both open and close-loop solutions for the above non-convex, yet flat Problem via SBOPT will be presented and analysed in Section V.

Once the rendezvous is achieved, the deployment of the robotic arm and the pre-capture phase start. This process is characterized by the interaction between the chaser's robotic end-effector with the RSO.

Motion planning for the end-effector is mainly conceived in two manners: either the chaser is assumed to be a free-flying body or free-floating [7]. In this communication, the latter approach is assumed, and the regulation of the centre-of-mass state is tasked to a secondary GNC loop. In the free-flying scenario, motion planning is fundamentally an inverse kinematics problem, see [7,85] and the references therein. In particular, the end-effector position and attitude shall be regulated to a given reference state, which describes that of the berthing device or port on the target spacecraft. Ultimately in this case, the following simplified problem holds

$$
\begin{aligned}
\min J = \int_{t_0}^{t_{\max}} \dot{\boldsymbol{q}}^T \dot{\boldsymbol{q}} \ \mathrm{d}t, \\
s.t. \quad \dot{\boldsymbol{q}} = \boldsymbol{u}, \\
\boldsymbol{q}(t_0) = \boldsymbol{q}^0, \\
J(\boldsymbol{q})\, \dot{\boldsymbol{q}} = [\dot{\boldsymbol{r}}_e, \boldsymbol{\omega}\,], \\
\boldsymbol{e}_f\big(t_f, \boldsymbol{q}\big) - \boldsymbol{s}_{\mathrm{ref}} = \mathbf{0}, \\
||\boldsymbol{\omega}||_\infty \leq \omega_{\max}, \\
||\dot{\boldsymbol{r}}_e||_\infty \leq v_{\max}, \\
||\dot{\boldsymbol{q}}||_\infty \leq \dot{q}_{\max}.
\end{aligned}
$$

The end-effector state vector is comprised by its internal, operational degrees of freedom (as a multi-body system) $\boldsymbol{q}$. For robotic arms, these are usually conformed by either linear displacements (in telescopic joints) or 1 DoF angles (for revolute joints) [85]. The dynamics in play are dictated by the robot Jacobian J, which maps the internal velocities $\dot{\boldsymbol{q}}$ with those in the task space (linear $\dot{\boldsymbol{r}}_e$ and angular $\boldsymbol{\omega}$ velocity, up to some transformation). Such linear map may be constructed systematically by means of the robot homogeneous transformation matrices $R(\boldsymbol{q}) \in \mathrm{SE}(3)$ provided, for example, by the Denavit–Hartenberg (DH) parameters [85]. The capture shall be accomplished in a fixed time $t_{\max}$. The initial state of the end-effector is given by the final conditions on the close-range rendezvous (pre-deployment state), while the final boundary conditions are imposed by the target docking port $\mathbf{s}_{\mathrm{ref}}$ at the capture epoch through a nonlinear transformation $\boldsymbol{e}_f(\boldsymbol{q}) - \mathbf{s}_{\mathrm{ref}} = \mathbf{0}$ (determined by the very same DH parameters). Both the end-effector linear $\dot{\boldsymbol{r}}_e$ and angular velocity $\boldsymbol{\omega}_e$ are mechanically and operatively upper-bounded, and so they are the operational internal velocities $\dot{\boldsymbol{q}}$. Note that this formulation is independent of the robot itself, as it proposes a purely kinematic solution.

IV. NMPC-RTI for Real Time Optimal Control

The real-time implementation of SBOPT as close-loop optimal control technique requires of an additional architecture in which to embed such guidance engine. In practice, both general measurement noise, unmodelled disturbances and both implementation errors and numerical considerations come into play in demising of the open-loop solutions provided by SBOPT. This is especially true for these missions when compared to traditional cooperative rendezvous and proximity operations, as the target's physical parameters may not be known accurately, and online identification is usually needed [7]. In this work, we use Nonlinear Model Predictive Control (NMPC) as a method to handle uncertainties in real mission cases.

MPC can be understood as a practical application of the more general Real Time Optimal Control (RTOC). In a broader sense, RTOC is comprised with the 'instantaneous' availability of optimal control laws [48, 86]. RTOC has only become computationally feasible for most applications after the first decade of the 21st century [4,48]. As for MPC, when deployed for processes of faster dynamics (greater Lipschitz constant [86]), usually only linear approximations or QP relaxations of the original optimal control problem are leveraged, to maintain the computational burden low. For nonlinear MPC (NMPC), these approaches generalizes into some iterative optimization technique, such as SQP or SCP. Still, when dealing with embedded applications, these techniques are not usually compliant with strict computational delay requirements. For such purpose, this communication advocates for a modified version of the standard Real-Time Iteration (RTI) scheme, which is described in detail in [87]. It shall be noticed that orbital motion is particularly well-suited for MPC deployments [34], as the typical time scales may

be considered to be slow. On the other hand, this is not applicable to attitude slews and motion planning, which shows considerably smaller characteristic times. As a result, a fast NMPC is needed when addressing the close-range rendezvous and the pre-capture phase, in which the end-effector is deployed.

Basically, in NMPC-RTI, a surrogate formulation of the problem at hands is solved through standard techniques (such as QP), but only for a single iterative pass (probably without convergence), with the latest information on the state of the system. The optimization process is warm-started with the shifted solution for the previous instant; in this way, only the initial iteration of the scheme requires of completing the optimization process. When compared to traditional RTI cores, our SBOPT algorithm replaces the standard QP solver as the inner guidance planner. The SBOPT collocation scheme, as described in Section III, employs a differential (not integral) form of the dynamics, and assumes differential flatness for the system, so that the configuration variables of the problem are the only needed solution (avoiding the need to store the control plan solution). Moreover, these are assumed to be polynomial, and initial guesses are naturally generated to comply with boundary conditions within the method. Most importantly, because it is lies on PS theory, it shows pseudospectral convergence [88], requiring of a small number of collocation points and polynomial degree to converge (exponentially under mild assumptions). However, this is usually against the Lipschitz constant of the system, and thus, against feasibility of the solution: less collocation points leads to aliasing between collocation nodes. In any case, even if the optimization is inexact (as in classical RTI), when compared to the standard architecture, our scheme is in this way more compact, requires of less memory and computational workload. All in all, it is particularly suited for embedded application, once an NLP solver is available.

In our NMPC scheme, OCP are iteratively solved and refreshed with new information of the system at a frequency of T_s. No assumptions are made regarding our control or prediction horizons, which may be selected to cover the full mission time span ($t_{\max}$). In general, we use a classical receding scheme. The optimization outputs a (general) rational polynomial (through applying the optimal configuration evolution $\mathbf{s}$ to the inverse dynamics equation), to be used as an open-loop controller as a function of the independent variable of the problem. This is implemented via functional decomposition on Legendre polynomials, leading to the map $t \mapsto \mathbf{u}(t)$.

During the synthesis of this new controller, the previous solution is used to steer the system until the new ones is available. The sampling time is thus the sum of the T_s period and the synthesis computational cost Δt. Moreover, in this way, a feasible solution is always available.

As a relevant remark, Problem (6) has its final boundary conditions open. This has severe implications on the feasibility of the NMPC scheme. In order to handle it, we include a Mayer term in the cost function penalizing deviations from previously computed boundary conditions (which are used as warm start), as if they were an equilibrium trajectory of the system [43].

V. Mission Applications

The following Section is dedicated to present practical examples of the above NMPC architecture. In particular, an integral berthing mission is design, from the rendezvous with the target to the pre-capture phase, finishing with the deployment and contact of a robotic manipulator with the target.

The OCP presented in Section III were intended to be computationally tractable. In practice, simulations consider unmodelled effects and disturbances to test the robustness of the approach. These include the effect of the J_2 acceleration in the orbital motion, as well as the osculaing LVLH frame of the target for the translational problem; in the attitude problem case, gravity gradient disturbances is also included into the analysis, as well as the appropriate inertial terms in the Euler-Poinsot system, avoided in the GNC model. Unmodelled uncertainty is introduced into the pre-capture phase via a spring-damper model for the joints, together with sinusoidal control errors. In all cases, initial conditions are corrupted with Gaussian noise without any navigation solution to filter it.

Simulations were completed in Matlab 2021b using an 11th Gen Intel(R) Core(TM) i7-1165G7 @ 2.80 GHz with 15.7 GB of RAM.

The mission starts with an uncoupled long-range rendezvous, in which the following reference state for the target shall be achieved-

$$\boldsymbol{\rho}(t_f) = 0,\ \dot{\boldsymbol{\rho}}(t_f) = 0,\ \boldsymbol{\sigma}(t_f) = \left[\tfrac{1}{3}, \tfrac{1}{3}, \tfrac{1}{3}\right],\ \boldsymbol{\omega}(t_f) = 0.$$

The control authority is bounded by 0.005 m/s^2 and 0.005 Nm for the chaser. The linear velocity is constrained to be less than 5 m/s and for angular case, 1 rad/s. The chaser inertia is given by $I = [1,2,3]$ in arbitrarily selected mass units. The initial conditions for the rendezvous are taken from [47], corresponding to a range of nearly 500 meters and rest attitude conditions.

The mission is to be accomplished in 1 hour, with a control sampling time of 10 seconds (thanks to the controller synthesis via SBOPT, when compared to

traditional 1s values [43]). The following figures demonstrate the rendezvous trajectory, as well as the associated control effort. The numerical MPC setup is given by $N = 7$ and $m = 30$, using Legendre polynomials and the LGL quadrature. In this case, both the orbital and attitude problems can be solved individually, as the feasible region of the problem uncouples the flat outputs of the system.

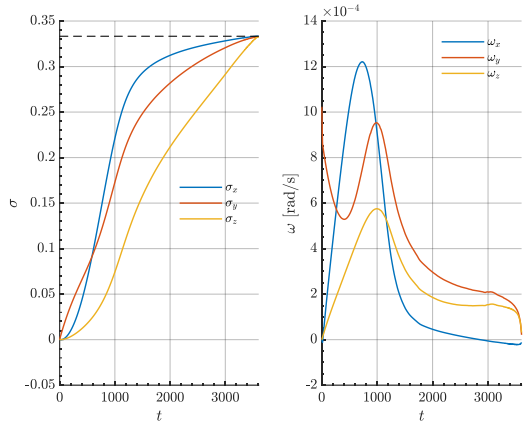

Figure 7. MPC Attitude state trajectory for the long-range rendezvous.

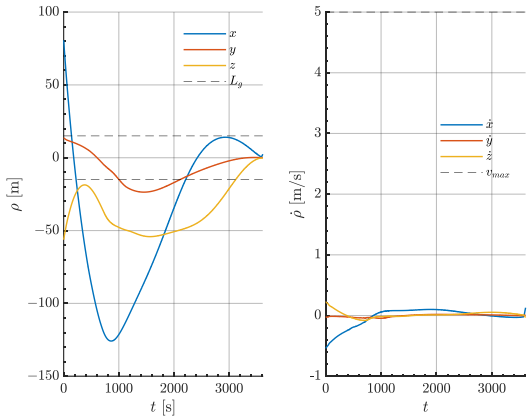

Figure 8. Relative position trajectory for the long-range rendezvous.

Note that, as the final time of flight approaches, the solver is not able to find reasonable control laws to achieve the last steps in the rendezvous, leading to unfeasible solutions for the control vector, see the next figure.

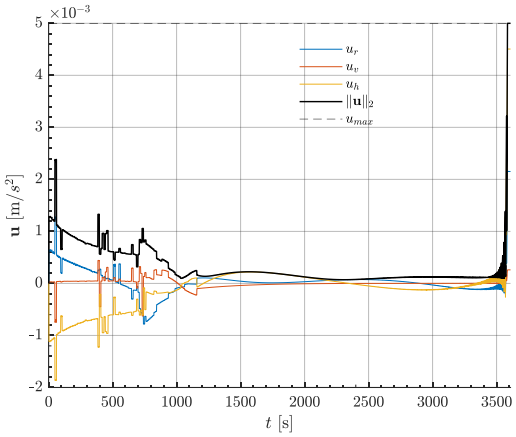

Figure 9. Control acceleration during the long-range rendezvous.

The coupled, close-range rendezvous follows this initial phase for the next 1800s. The remaining constraining parameters, as well as the target initial conditions, are given by [43], while the rest of the numerical setup is kept the same.

While the open-loop trajectory is satisfactorily optimized, being both feasible and at least being a local minimum, the computational load of the problem makes the deployment of the algorithm infeasible for fast rotating targets. The computational time taken by the solver, in the order of 10s, clearly exceeds the one needed by the intrinsic dynamics of the problem. Thus, the close-loop berthing problem remains an open line of research; in particular, the optimization of either the problem or the solver for this type of missions (note that the technique has been demonstrated previously for cooperative rendezvous, for which the above examples provide mild approximations).

Considering the rendezvous accomplished, a generic pre-capture phase is considered, characterized by the following reference end-effector state to be acquired by the robotic arm (linear position and attitude, parametrized by MRP). For simplicity, we take these refence states to be constant, although general reference trajectory tracking may be instead used.

$$\boldsymbol{r}_{\text{ref}} = [0.2, -0.05, 0.01\,]^T \text{ m}, \qquad \boldsymbol{v}_{\text{ref}} = \boldsymbol{0}\,\frac{\text{m}}{\text{s}},$$

$$\boldsymbol{\sigma}_{\text{ref}} = [0.33, 0.01, 0.33]^T, \ \boldsymbol{\omega}_{\text{ref}} = 5\,\boldsymbol{k}\,\frac{\text{rad}}{\text{s}}.$$

The robotic arm used follows the physical design of UR3e [89], from which its DH parameters are available. The capture shall be achieved in a total of 300 s, with a refresh rate of $T_s = 2$ s. Both the prediction and control horizons are set as 300 s. The problem is constrained via $\omega_{\max} = 20\,\frac{\text{deg}}{\text{s}}$, $v_{\max} = 2\,\frac{\text{m}}{\text{s}}$ and $\dot{\boldsymbol{q}}_{\max} = 180\,\frac{\text{deg}}{\text{s}}$.

The solver is set with a maximum polynomial order of $N = 5$ and $m = 20$ LGL quadrature points, while Legendre polynomials are used. The computational cost of each optimization can be analysed in the following figure.

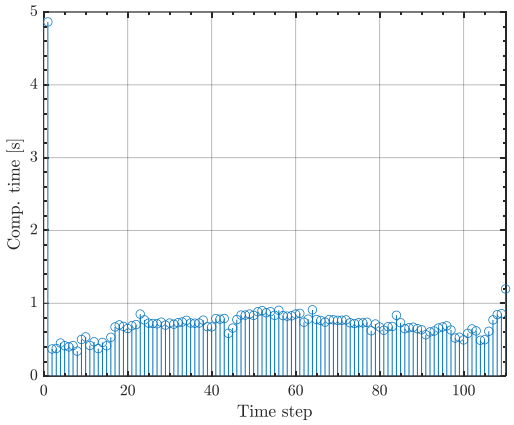

Figure 10. Computational time versus NMPC iteration for the manipulator problem.

Once the initial optimization is completed, the computational time is safely under the T_s frequency, remaining steadily all throughout the operation of the robot.

Gaussian noise is added to each of the joint angle measurements at each iteration, with diagonal covariance matrix characterized by the following standard deviation $\boldsymbol{\sigma}_q^2 = 0.01\ \text{deg}^2$.

The following Figures summarize the results obtained, showing that the end-effector achieves the reference state at the final epoch. No constraint violation is found across the simulation.

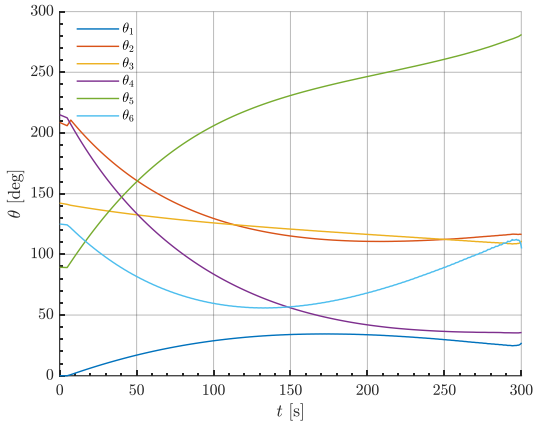

Figure 11. NMPC trajectory in the joints space.

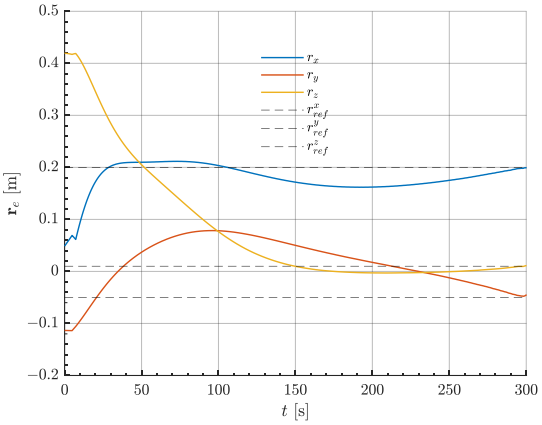

Figure 12. NMPC end-effector position trajectory.

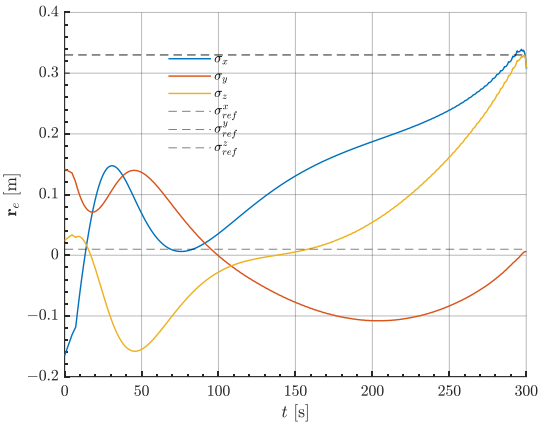

Figure 13. NMPC attitude (MRP) end-effector trajectory.

VI. Hardware In the Loop Campaign

Final validation and verification of the proposed guidance and control architecture is achieved through a Hardware in the Loop campaign (HIL) at the University Rey Juan Carlos SPOL laboratory.

Verification and validation simulations were carried out for the very two different phases in which the berthing mission has been divided. Figs. 14 to 16 graphically compiles the tracking performance of the algorithm, together with the end-effector position and attitude, as commanded by the NMPC-RTI scheme, for a pre-capture phase example.

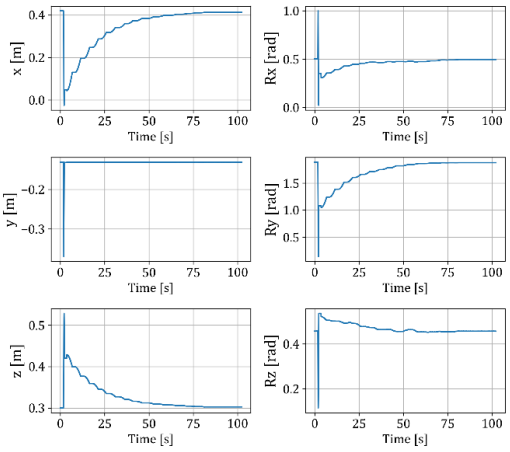

Figure 14. Example of HIL pre-capture phase onboard a 6 DoF robotic arm (end-effector space).

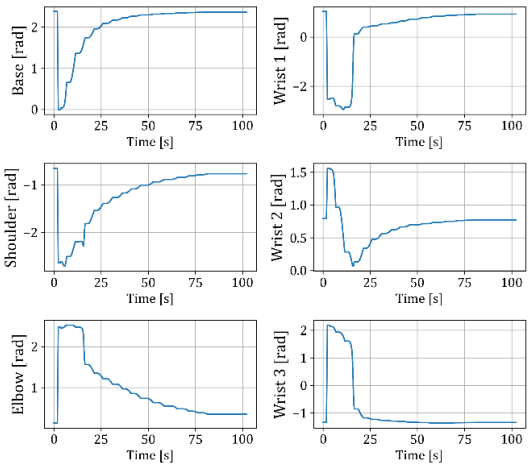

Figure 15. Example of HIL pre-capture phase onboard a 6 DoF robotic arm (joint space).

Figure 16. Robotic arm and end-effector during the pre-capture phase.

VII. CONCLUSIONS

The optimal design of general berthing missions, from start (long-range rendezvous) to end (pre-capture phase), is studied in this communication through the lens of computational Real Time Optimal Control. Building on previous results, this paper extends open-loop trajectory optimization to an NMPC-RTI architecture capable of close-loop, online guidance and control.

First, we explore the benefits and flaws of a novel generic optimal control solver, both from a theoretical and practical perspective. Special attention is risen towards its online computational capabilities. Once its capabilities are shown within classical OCP examples, the algorithm is systematically applied as the guidance engine in charge of designing the optimal berthing missions of interest. Moreover, to close the loop and proposed a complete guidance and control architecture, this novel optimization engine is combined with a NPMC scheme. The solver is shown to have great synergies with such design, especially interesting for embedded GNC applications onboard real hardware. Both Model and Hardware in the Loop campaigns are introduced to analyse the proposed architecture.

Despite the results obtained, several lines of research remain open and may be discussed. Primarily, these root in the theoretical foundations upon which the solver is constructed. As examples, exact convergence proofs are still to be developed, and the global optimality of solutions cannot be verified at the current stage; feasibility and stability of the NMPC loop cannot be also guaranteed. In this sense, the hybridization of the solver design with classical optimal control techniques (such as PMP) appears promising. By the time of writing this communication, the authors aim the solver foundations to root in the newborn field of Hamiltonian Programming (in contrast to traditional NLP), to formally exploit the particular mathematical structure of Optimal Control Problem for practical applications.

VIII. REFERENCES

[1] Kessler, D.J., “Collisional cascading: The limits of population growth in low earth orbit”, Advances in Space Research, pp. 63-66, 1991.

[2] Shan, M. and Guo, J. and Gill, E., “Review and comparison of active space debris capturing and removal methods”, Progress in Aerospace Sciences, pp. 18-32, 2016.

[3] Flores-Abad, A. and Ma, O. and Pham, K. and Ulrich, S., “A review of space robotics technologies for on-orbit servicing”; Progress in Aerospace Sciences, pp. 1-26, 2014.

[4] Ross, I.M. and Karpenko, M., “A review of pseudospectral optimal control: From theory to flight”, Annual Reviews in Control, pp. 182-197, 2012.

[5] Mcknight, D. and Di Pentino, F., Kaczmarek and A. and Knowles, S., “Detumbling Rocket Bodies in Preparation for Active Debris Removal”; Proceedings of the 6th European Conference on Space Debris, 2013.
[6] Castronuovo, M. M., “Active space debris removal—A preliminary mission analysis and design”, Acta Astronautica, 2011.
[7] Moghaddam, B. M. and Chhabra, R., “On the guidance, navigation and control of in-orbit space robotic missions: A survey and prospective vision”, Acta Astronautica, pp. 70-100, 2021.
[8] Agrawal, O.P. and Xu, Y., “On the global optimum path planning for redundant space manipulators”, IEEE Transactions on Systems, Man, and Cybernetics, pp. 1306-1316,1994.
[9] Papadopoulos, E. and Abu-Abed, A., “Design and motion planning for a zero-reaction manipulator”, Proceedings of the 1994 IEEE International Conference on Robotics and Automation, 1994.
[10] Lampariello, R. and Agrawal, S. and Hirzinger, G., “Optimal motion planning for free-flying robots”, 2003 IEEE International Conference on Robotics and Automation, 2003.
[11] Aghili, F., “Optimal Control for Robotic Capturing and Passivation of a Tumbling Satellite with Unknown Dynamics”, AIAA Guidance, Navigation and Control Conference and Exhibit, 2008.
[12] Aghili F.. "Automated Rendezvous & Docking (AR&D) without Impact Using a Reliable 3D Vision System," AIAA 2010-7602. AIAA Guidance, Navigation, and Control Conference, 2010.
[13] Boyarko, G., “*Spacecraft Guidance Strategies for Proximity Maneuvering and Close Approach with a Tumbling Object*”, Naval Postgraduate School, 2010.
[14] Boyarko, G. and Yakimenko, O. and Romano, M., “Optimal Rendezvous Trajectories of a Controlled Spacecraft and a Tumbling Object”, Journal of Guidance, Control, and Dynamics, pp. 1239-1252, 2011.
[15] Michael, J. and Chudej, K. and Gerdts, M. and Pannek, J., “Optimal Rendezvous Path Planning to an Uncontrolled Tumbling Target”, Automatic Control in Aerospace, pp. 347-352, 2013.
[16] Wilde, M. and Ciarcià, M. and Grompone, A. and Romano, M., “Experimental Characterization of Inverse Dynamics Guidance in Docking with a Rotating Target”, pp. 1173-1187, 2016.
[17] Biggs, J. and Caubet, A. “An Inverse Dynamics Approach to the Guidance of Spacecraft in Close Proximity of Tumbling Debris”, 2015.
[18] Stoneman, S. and Lampariello, R., “A Nonlinear Optimization Method to Provide Real-Time Feasible Reference Trajectories to Approach a Tumbling Target Satellite”, 2016.
[19] Ventura, J., Ciarcia, M., Romano, M. and Walter, U., "An Inverse Dynamics-Based Trajectory Planner for Autonomous Docking to a Tumbling Target," AIAA 2016-0876. AIAA Guidance, Navigation, and Control Conference. January 2016.
[20] Virgili-Llop, J. and Zagaris, C. and Zappulla II, R. and Bradstreet, A. and Romano, M., “Convex Optimization for Proximity Maneuvering of a Spacecraft with a Robotic Manipulator”, Proceedings of the 27th AAS/AIAA Spaceflight Mechanics Meeting, 2017.
[21] Flores-Abad, A. and Zhang, L. and Wei, Z. and Ma, O., “Optimal Capture of a Tumbling Object in Orbit Using a Space Manipulator”, Journal of Intelligent and Robotic Systems, pp. 199-211, 2017.
[22] Sternberg, D, “*Optimal docking to tumbling objects with uncertain properties*”, 2017.
[23] Zagaris, C. and Romano, M., “Applied Reachability Analysis for Spacecraft Rendezvous and Docking with a Tumbling Object”, 2018 Space Flight Mechanics Meeting, 2018.
[24] Xu, Z. and Chen, Y. and Xu, Z., “Optimal guidance and collision avoidance for docking with the rotating target spacecraft”, Advances in Space Research, pp. 3223-3234, 2019.
[25] Abdollahzadeh, P. and Esmailifar, S.M, “Automatic orbital docking with tumbling target using sliding mode control”, Advances in Space Research, pp. 1506-1525¸2021.
[26] Dong, K. and Luo, J. and Dang, Z. and Wei, L, “Tube-based robust output feedback model predictive control for autonomous rendezvous and docking with a tumbling target”, Advances in Space Research, pp. 1158-1181, 2020.
[27] Specht, C., Bishnoi, A., and Lampariello, R., “Autonomous Spacecraft Rendezvous Using Tube-Based Model Predictive Control: Design and Application”, Journal of Guidance, Control, and Dynamics, 2023.
[28] Buckner, C. and Lampariello, R., “Tube-based model predictive control for the approach maneuver of a spacecraft to a free-tumbling target satellite”; 2018 Annual American Control Conference (ACC), 2018.
[29] Santos, R.R. and Rade, D.A. and {da Fonseca}, I. M.., “A machine learning strategy for optimal path planning of space robotic manipulator in on-orbit servicing”, Acta Astronautica, 2022.
[30] Zhang, O. and Yao, W. and Du, D. and Wu, C. and Liu, J. and Wu, L. and Sun, Y., “Trajectory optimization and tracking control of free-flying space robots for capturing non-cooperative tumbling objects”, Aerospace Science and Technology, 2023.
[31] Richards, A. and How, J., “Performance Evaluation Of Rendezvous Using Model Predictive Control”, AIAA Guidance, Navigation, and Control Conference and Exhibit, 2003.
[32] Breger, L. and How, J., “J2-modified GVE-based MPC for formation flying spacecraft”, 2012.
[33] Gavilán, F. and Vázquez, R. and Camacho, E. F., “Chance-constrained model predictive control for

spacecraft rendezvous with disturbance estimation", Control Engineering Practice, 2012.
[34] Hartley, E. N., "A tutorial on model predictive control for spacecraft rendezvous", 2015 European Control Conference (ECC), 2015.
[35] Richards, A. and How, J., "Analytical Performance Prediction for Robust Constrained Model Predictive Control", International Journal of Control, 2006.
[36] Mammarella, M. and Capello, E. and Guglieri, G., "Robust Model Predictive Control for Automated Rendezvous Maneuvers in Near-Earth and Moon Proximity", 2018.
[37] Leomanni, M. and Bianchini, G. and Garulli, A. and Giannitrapani, A. and Quartullo, R., "Sum-of-Norms Model Predictive Control for Spacecraft Maneuvering", IEEE Control Systems Letters, 2019.
[38] Sánchez, J. and Gavilán, F. and Vázquez, R., "Chance-constrained Model Predictive Control for Near Rectilinear Halo Orbit Spacecraft Rendezvous", Aerospace Science and Technology, 2020.
[39] Pagone, M. and Boggio, M. and Novara, C. and Vidano, S., "A Pontryagin-based NMPC approach for autonomous rendez-vous proximity operations", 2021 IEEE Aerospace Conference (50100), 2021.
[40] Capannolo, A. and Zanotti, G. and Lavagna, M. and Cataldo, G., "Model predictive control for formation reconfiguration exploiting quasi-periodic tori in the cislunar environment", Nonlinear Dynamics, 2023.
[41] Pagone, M., Bucchioni, G., Alfino, F. and Novara, C., "A Minimum-propellant Pontryagin-based Nonlinear MPC for Spacecraft Rendezvous in Lunar Orbit: the Extended Version", 2023.
[42] Oestreich, C.E., Linares, R. and Gondhalekar, R., "Tube-based model predictive control with uncertainty identification for autonomous spacecraft maneuvers", Journal of Guidance, Control, and Dynamics, 2023.
[43] Rebollo, J.A., Vázquez, R, Alvarado, I., Limón, D., "MPC for Tracking applied to rendezvous with non-cooperative tumbling targets ensuring stability and feasibility", 2024.
[44] Tschauner, J., and Hempel, P., "Rendezvous zu einemin Elliptischer Bahn Umlaufenden Ziel", Acta Astronautica, pp. 104-109, 1965.
[45] Schaub, H. and Junkins, J., "Stereographic Orientation Parameters for Attitude Dynamics: A Generalization of the Rodrigues Parameters". Journal of the Astronautical Sciences, 44, 1995.
[46] Solano-López, P. and Cuevas del Valle, S. and Solá, A. and Urrutxua, H., "An investigation on shape-based methods with different polynomial basis for low-thrust mission design", Proceedings of the 9th European Conference For Aeronautics And Space Sciences (EUCASS), 2022.
[47] Cuevas del Valle, S., Velázquez Navarro, E., Solano-López, P. and Urrutxua, H., "A differentially-flat, pseudospectral, shape-based solver and embedded MPC for berthing with non-cooperative targets", AIAA Scitech 2024 Forum, 2024.
[48] Ross, I.M, "*A primer on Pontryagin's Principle in Optimal Control*", 2015.
[49] Rao, A., "A Survey of Numerical Methods for Optimal Control", Advances in the Astronautical Sciences, 135, 2010.
[50] Ross, I., "A historical introduction to the covector mapping principle"; Advances in the Astronautical Sciences, 123, 2006.
[51] Ross, I.M, "A Direct Shooting Method is Equivalent to an Indirect Method", 2020.
[52] Ross, I.M., "Enhancements to the DIDO© Optimal Control Toolbox", 2020.
[53] Karpenko, M. et al., "Fast Attitude Maneuvers for NASA's Lunar Reconnaissance Orbiter: Practical Flight Application of Attitude Guidance using Birkhoff Pseudospectral Theory and Hamiltonian Programming," in IEEE Control Systems Magazine, vol. 44, no. 2, pp. 26-54, April 2024, doi: 10.1109/MCS.2024.3358593.
[54] Ross, I.M. and Fahroo, F., "Legendre Pseudospectral Approximations of Optimal Control Problems", 2004.
[55] Fahroo, F. and Ross, I.M., "Direct trajectory optimization by a Chebyshev pseudospectral method", Proceedings of the 2000 American Control Conference, 2000.
[56] Garg, D. and Hager, W. W. and Rao, A. V., "Pseudospectral methods for solving infinite-horizon optimal control problems", Automatica, 2011.
[57] Petropoulos, A.E. and Longuski, J.M., "Shape-Based algorithm for automated design of low-thrust, gravity-assist trajectories", Journal of Spacecraft and Rockets, 2004.
[58] Izzo, D., "Electric sail trajectory design with Bezier curve-based shaping approach", Journal of Guidance, Control, and Dynamics, 2006.
[59] Wall, B. and Conway, B., "Shape-based approach to low-thrust rendezvous trajectory design", Journal of Guidance, Control, and Dynamics, 2009.
[60] Abdelkhalik, O. and Taheri, E., "Approximate on-off low-thrust space trajectories using Fourier series", Journal of Spacecraft and Rockets, 2012.
[61] Roa, J. and Peláez, J. and Senent, J., "New analytic solution with continuous thrust: generalized logarithmic spirals", 2016.
[62] Xie, C. and Zhang, G. and Zhang, Y., "Shaping approximation for low-thrust trajectories with large out-of-plane motion", Journal of Guidance, Control, and Dynamics, 2016.
[63] Huo, M. and Mengali, G. and Quarta, A. and Qi, N., "Electric sail trajectory design with Bezier curve-based shaping approach", Aerospace Science and Technology, 2019.
[64] Fan, Z. and Huo, M. and Qi, N. and Zhao, C. and Yu, Z. and Lin, T., "Initial design of low-thrust

trajectories based on the B\'ezier curve-based shaping approach", 2020.
[65] Trefethen, L. N., "*Spectral Methods in MATLAB*", Society for Industrial and Applied Mathematics (SIAM), 2000.
[66] Trefethen, L. N., "Is Gauss Quadrature Better than Clenshaw–Curtis?", SIAM Review, 2008.
[67] Fahroo, F. and Ross, I., "Second Look at Approximating Differential Inclusions", Journal of Guidance Control and Dynamics, 2001.
[68] Petit, N. and Milam, M.B. and Murray, R. M., "Inversion Based Constrained Trajectory Optimization", 5th IFAC Symposium on Nonlinear Control System, 2001.
[69] Ross, I.M. and Fahroo, F., "Pseudospectral methods for optimal motion planning of differentially flat systems", Proceedings of the 41st IEEE Conference on Decision and Control, 2002.
[70] Ross, I.M. and Fahroo, F., "A unified computational framework for real-time optimal control", 42nd IEEE International Conference on Decision and Control, 2003.
[71] Herman, A. L. and Conway, B. A., "Direct optimization using collocation based on high-order Gauss-Lobatto quadrature rules", Journal of Guidance, Control, and Dynamics, 1996.
[72] Mathworks, "fmincon", https://es.mathworks.com/help/optim/ug/fmincon.html. Online, accessed 04th July 2023
[73] Betts, J. T., "*Practical Methods for Optimal Control and Estimation Using Nonlinear Programming*", Society for Industrial and Applied Mathematics, 2010.
[74] Ross, I. M. and Rea, J. R. and Fahroo, F., "Exploiting Higher-order Derivatives in Computational Optimal Control", Proceedings of the 10th Mediterranean conference on Control and Automation, 2002.
[75] Koeppen, N. and Ross, I. and Wilcox, L. and Proulx, R., "Fast Mesh Refinement in Pseudospectral Optimal Control", 2019.
[76] Ross, I.M., "A Universal Birkhoff Theory for Fast Trajectory Optimization", 2023.
[77] Proulx, R.J. and Ross, I.M., "Implementations of the Universal Birkhoff Theory for Fast Trajectory Optimization", 2023.
[78] embotech, "ECOS: Embedded Conic Solver", https://github.com/embotech/ecos/wiki, 2023. Online, accessed: 20th November 2023.
[79] Reynolds, T. P. and Mesbahi, M., "The Crawling Phenomenon in Sequential Convex Programming", 2020.
[80] Malyuta, D. et al., "Convex Optimization for Trajectory Generation: A Tutorial on Generating Dynamically Feasible Trajectories Reliably and Efficiently," in IEEE Control Systems Magazine, vol. 42, no. 5, pp. 40-113, Oct. 2022.
[81] Louembet, C., and Deaconu, G., "Collision avoidance in low thrust rendezvous guidance using flatness and positive B-splines", Proceedings of the 2011 American Control Conference, 2011.
[82] Fliess, M., Lévine, J., Martin, P., and Rouchon, P., "On differentially flat nonliear systems", Proc. 2nd. IFAC NOLCOS Symposium Bordeaux, 1992.
[83] Clohessy, W. H. and Wiltshire, R. S., "Terminal Guidance System for Satellite Rendezvous", Journal of the Aerospace Sciences, 1960.
[84] Louembet, C., "Generation de Trajectoires Optimales Pour Systèmes Differentiellment Plats: Application Aux Manoeuvres d'Attitude Sur Orbite", L'Université Bordeaux I, 2007.
[85] Siciliano, B. and Sciavicco, L. and Oriolo, G., "*Robotics: Modelling, Planning and Control*", Springer, 2009.
[86] Ross, I. and Sekhavat, P. and Fleming, A. and Gong, Q., "Optimal Feedback Control: Foundations, Examples, and Experimental Results for a New Approach", Journal of Guidance, Control, and Dynamics, 2008.
[87] Gros, S. and Zanon, M. and Quirynen, R. and Bemporad, A. and Diehl, M., "From linear to nonlinear MPC: bridging the gap via the real-time iteration", International Journal of Control, 2016.
[88] Gong, Q., Ross, I. and Kang, W. and Fahroo, F., "Connections between the covector mapping theorem and convergence of pseudospectral methods", Computational Optimization and Applications, 2008.
[89] Universal Robots, "UR3e", Online; accessed 16th April 2024.